S-wave kinematics in acoustic transversely isotropic media with a vertical symmetry axis

S.Jin* & A.Stovas

Affiliation: Norwegian University of Science and Technology (NTNU), Department of Geoscience and Petroleum, S. P. Andersens veg 15a, 7031 Trondheim, Norway

*Email: jin.song@ntnu.no;

Abstract

Acoustic transversely isotropic models are widely used in seismic exploration for P-wave processing and analysis. In isotropic acoustic media only P-wave can propagate, while in an acoustic transversely isotropic medium both P- and S-waves propagate. In this paper, we focus on kinematic properties of S-wave in acoustic transversely isotropic media. We define new parameters better suited for S-wave kinematics analysis. We also establish the traveltime and relative geometrical spreading equations and analyse their properties. To illustrate the behaviour of the S-wave in multi-layered acoustic transversely isotropic media, we define the Dix-type equations that are different from the ones widely used for the P-wave propagation.

Keywords

Acoustics, Anisotropy, Modelling, Kinematics

Introduction

For an elastic transversely isotropic medium with vertical symmetry axis (VTI), the qP- and qSV-wave parameters are defined by Thomsen (1986): the vertical P- and S-wave phase velocities v_{P0} and v_{S0} and two anisotropy parameters ε and δ. Later, Tsvankin and Thomsen (1994), Alkhalifah and Tsvankin (1995) and Alkhalifah (1998) showed that qP-wave kinematical property is insensitive to the parameter v_{S0} with practical weak anelliptic parameter defined as $\eta = (\varepsilon - \delta)/(1+2\delta)$. Thus, assuming $v_{S0} = 0$ reduces the variables and facilitates the analysis of qP-wave kinematic properties. That results in a new parameterization including vertical and NMO P-wave velocities v_{P0} and $v_{Pn} = v_{P0}\sqrt{1+2\delta}$ and anelliptic parameter η (Alkhalifah and Tsvankin 1995). The medium defined by this set of parameters is called the acoustic VTI medium (Alkhalifah 1998).

However, in acoustic VTI medium, there is also the diamond shaped S-wave that propagates (Fig. 1), which can be considered as unwanted artifacts (Grechka, Zhang and Rector III 2004). In order to eliminate this artifact in seismic modelling, Alkhalifah (2000) proposed to add an isotropic acoustic medium as the top layer. Nevertheless, this method brings redundant multiples, and geophysicists further proposed various procedures to get rid of these concomitants in modelling of P-wave (Zhang, Rector III and Hoversten 2003; Han and Wu 2005; Zhou, Zhang and Bloor 2006; Hestholm 2009). Grechka *et al*. (2004) pointed out that the acoustic VTI medium can also be defined as an effective medium from the upscaling of the stack of isotropic or VTI layers if one or more layers are fluid ones. The corresponding effective medium defined by Backus averaging (Backus 1962) has the S-wave vertical phase velocity $v_{S0} = 0$ and turns out be a physical acoustic VTI medium (Appendix D). Another example of an anisotropic fluid is a liquid crystal (Chandrasekhar 1992).

In this paper, we revisit the acoustic VTI medium and focus on the kinematical properties of S-wave. In elastic VTI medium, equations for slowness surfaces of qP- and qSV-waves are coupled. Setting $v_{S0} = 0$ results in decoupling of these equations, and remained equation is typically used to describe P-wave propagation only. We show that this equation also describes S-wave but is defined in a completely different range of horizontal slowness. The new parameterization for S-wave is defined based on the slowness surface branch corresponding to S-wave. The traveltime and relative geometrical spreading equations are also derived for S-wave in acoustic VTI medium. An extension to the multi-layered medium is defined by applying the Dix-type equations, that are different from those defined for P-wave.

The slowness surface in acoustic VTI media

For elastic VTI media with the S-wave vertical phase velocity $v_{S0} > 0$, the vertical slowness q for qP- and qSV-waves can be found from the solution of Christoffel equation as a function of horizontal slowness p (Appendix A),

$$q = \sqrt{\frac{-2c}{b \pm \sqrt{b^2 - 4ac}}}, \tag{1}$$

with a, b and c defined by v_{P0}, v_{S0}, v_{Pn} and η,

$$\begin{aligned} a &= v_{S0}^2 v_{P0}^2, \\ b &= v_{S0}^2[p^2(v_{Pn}^2 + v_{P0}^2) - 1] + v_{P0}^2(2\eta v_{Pn}^2 p^2 - 1), \\ c &= (p^2 v_{S0}^2 - 1)[(1+2\eta)v_{Pn}^2 p^2 - 1]. \end{aligned} \tag{2}$$

Equation (1) is coupled, and positive and negative signs correspond to qSV- and qP-waves, respectively. The qP-wave horizontal slowness range is given by(Appendix A)

$$0 \le p \le \frac{1}{v_{Pn}\sqrt{1+2\eta}}. \tag{3}$$

If there is no qSV-wave horizontal triplication, the range of horizontal slowness for qSV-wave can be written as (Appendix A)

$$0 \le p \le \frac{1}{v_{S0}}. \tag{4}$$

The qSV-wave horizontal slowness can be larger than $1/v_{S0}$ if the horizontal triplication exists (Appendix A).

For the acoustic VTI medium, $v_{S0}=0$ and $\eta \ge 0$ (a stability criteria (Alkhalifah 2000)), the P- and S-waves slowness surface equation is given by (Appendix A),

$$q = \frac{1}{v_{P0}}\sqrt{\frac{(1+2\eta)v_{Pn}^2 p^2 - 1}{2\eta v_{Pn}^2 p^2 - 1}}. \tag{5}$$

Equation (5) is widely used for P-wave propagation in acoustic VTI media (Alkhalifah 1998), and P-wave horizontal slowness range is also given by equation (3). However, equation (5) also describes the S-wave propagation within the range of horizontal slowness (Appendix A),

$$\frac{1}{v_{Pn}\sqrt{2\eta}} \le p \le +\infty. \tag{6}$$

The slowness surface given by equation (5) is shown in Fig. 2 with separated branches corresponding to P- and S-waves. The P-wave slowness surface in the acoustic case is very similar to the elastic one of the quasi-elliptical shape. The S-wave slowness surface in the acoustic case is quasi-hyperbolic with two asymptotes given by (Appendix A)

$$p = \frac{1}{v_{Pn}\sqrt{2\eta}}, \tag{7}$$

and

$$q = \frac{1}{v_{P0}} \sqrt{\frac{1+2\eta}{2\eta}} \,. \tag{8}$$

The P- and S-waves group angles (taken from the vertical direction) as functions of horizontal slowness are given in equation (B4) with distinctive horizontal slowness ranges as in equations (3) and (6). We plot P- and S-wave phase angle — group angle relationships for an acoustic VTI medium in Fig. 3a. The model parameters are listed in Table 1. One can note that the P-wave group angle increases with the phase angle. When the horizontal slowness $p = 0$, the P-wave phase angle and group angle are both zero. When the horizontal slowness $p = 1/(v_{Pn}\sqrt{1+2\eta})$, the P-wave phase angle and group angle are 90 degree. However, the S-wave group angle decreases with the increase of its phase angle. The lower limit of horizontal slowness ($p = 1/(v_{Pn}\sqrt{2\eta})$) corresponds zero phase angle and 90 degree group angle, and the upper limit ($p = +\infty$) is related to S-wave ray in the vertical direction with phase angle being 90 degree. We also calculate P- and S-waves polarization angles (taken from the vertical direction) as the functions of horizontal slowness (equation (A30)). For the model with parameters listed in Table 1, the P- and S-waves polarization angle – group angle relationships are demonstrated in Fig. 3b. One can see their polarization angles both increase with the group angle. Particularly, in the vertical or horizontal direction, the S-wave polarization angle is same with that for P-wave, and this is in consistence with the results in Grechka *et al*. (2004).

If η is zero, the S-wave does not exist with P-wave parameterization. Since $\eta > 0$, S-wave and P-wave slowness surfaces are not overlapped and have a gap in the horizontal slowness range given by (Appendix A; Fig. 2)

$$\frac{1}{v_{Pn}\sqrt{1+2\eta}} < p < \frac{1}{v_{Pn}\sqrt{2\eta}} \,. \tag{9}$$

Since the evanescent waves are ignored in this paper, for acoustic transversely isotropic media with vertical symmetry axis, in practice there is no wave mode conversion between reflected/transmitted P- and S-waves at the interface between two acoustic VTI layers ($v_{Pn,j}\sqrt{1+2\eta_j} > v_{Pn,k}\sqrt{2\eta_k}$, where *j* and *k* indicate the layer indices).

S-wave parameterization in an acoustic VTI medium

The vertical and horizontal S-wave group velocities V_{S0} and V_{SX} in acoustic VTI medium can be defined as (Appendix B),

$$V_{S0} = v_{P0}\sqrt{\frac{2\eta}{1+2\eta}}, \quad V_{SX} = v_{Pn}\sqrt{2\eta}\,. \tag{10}$$

Therefore, the new set of parameters suitable to describe the S-wave propagation is the following: V_{S0} , V_{SX} and η . Substituting S-wave parameters given in equation (10) into equation (5) results in a new equation for slowness surface in the acoustic VTI medium,

$$q = \frac{1}{V_{S0}}\sqrt{\frac{p^2V_{SX}^2 + 2\eta(p^2V_{SX}^2 - 1)}{(1+2\eta)(p^2V_{SX}^2 - 1)}}\,. \tag{11}$$

Note that the functional form of equations (5) and (11) is exactly the same. The S-wave horizontal slowness range can be defined from equation (11) as

$$\frac{1}{V_{SX}} \le p \le +\infty\,. \tag{12}$$

When $\eta = 0$, equation (11) reduces to

$$q = \frac{1}{V_{S0}}\sqrt{\frac{p^2V_{SX}^2}{p^2V_{SX}^2 - 1}}\,. \tag{13}$$

Equation (13) provides a reference medium for the S-wave propagation. It might be a little confusing that the $\eta = 0$ leads V_{S0} and V_{SX} in equation (10) to be zero, but what should be noted is that equations (11) and (13) are functions of the newly defined S-wave parameters (V_{S0}, V_{SX} and η) instead of the previous P-wave parameters (v_{P0}, v_{Pn} and η) in equation (5). The two sets of parameters should not be mixed.

The S-wave group velocity surface

The S-wave group velocity V_G and group angle φ (taken from the vertical symmetry axis) can be defined from the slowness surface as (Appendix B)

$$\frac{1}{V_G} = \frac{q - p\dfrac{dq}{dp}}{\sqrt{1+(\dfrac{dq}{dp})^2}}, \quad \tan\varphi = -\frac{dq}{dp}. \tag{14}$$

Substituting equation (11) into equation (14) gives the quasi-astroidal form group velocity surface (Fig. 1; Fig. 4a). One can note although the S-wave phase velocity is zero in the vertical and horizontal directions, its group velocity is non-zero for arbitrary group angle. In order to analyze the reference medium ($\eta = 0$), we substitute equation (13) into equation (14) and derive the explicit equation for group velocity surface given by the astroidal shape (Appendix B),

$$\frac{1}{V_G^{2/3}} = \frac{\sin^{2/3}\varphi}{V_{SX}^{2/3}} + \frac{\cos^{2/3}\varphi}{V_{S0}^{2/3}}. \tag{15}$$

The group velocity surfaces for P- and S-waves for a homogeneous acoustic VTI medium are shown in Fig. 4a. The medium parameters used in computation are listed in Table 1. The group velocity surfaces for P- and S-waves in case of $\eta = 0$ are also shown in Fig. 4a for comparison. Note the difference between P- and S-waves with corresponding parameterizations in case of

$\eta = 0$. The group velocity surfaces for P- and S-waves have elliptical and astroidal shapes, respectively. With increasing η, the P-wave group velocity decreases, while the S-wave group velocity increases.

The S-wave group velocity surface is given by continuous function with cusps located at both symmetry axes. The P- and S-wave group velocity surfaces are respectively convex and concave functions,

$$\begin{aligned} \text{P-wave}: \ & \frac{d^2 V_G}{d\varphi^2} < 0, \\ \text{S-wave}: \ & \frac{d^2 V_G}{d\varphi^2} > 0. \end{aligned} \tag{16}$$

P- and S-wave group velocity surfaces have the curvatures of different signs, and this indicates S-wave traveltime is represented by one branch of a triplication (Appendix B).

The S-wave traveltime equation

We first derive the S-wave traveltime equation in a homogeneous acoustic VTI medium with the new parameterization, followed by an extension to the multi-layered medium. In a homogeneous acoustic VTI medium, the S-wave source-receiver offset and two-way traveltime parametric equations are given by (Stovas and Fomel 2012)

$$\begin{aligned} x(p) &= -2z\frac{dq}{dp}, \\ t(p) &= px + 2qz, \end{aligned} \tag{17}$$

where z is the thickness of the layer. The limited series for traveltime in power of 2/3 as a function of offset can be computed from equation (17) (Appendix C),

$$t^{2/3}(\tilde{x}) = t_{S0}^{2/3}\left(1 + \tilde{x}^{2/3} + \frac{2}{3}\eta\tilde{x}^{4/3} + ...\right), \tag{18}$$

where the zero offset two-way traveltime $t_{S0} = 2z / V_{S0}$, the S-wave normalized offset $\tilde{x} = x / (t_{S0} V_{Sn})$, the S-wave NMO velocity

$$V_{Sn} = V_{SX}\sqrt{1+2\eta} = v_{Pn}\sqrt{2\eta(1+2\eta)}\,. \tag{19}$$

For the reference medium with $\eta = 0$, equation (18) reduces to the simple moveout equation

$$t^{2/3}(\tilde{x}) = t_{S0}^{2/3}(1+\tilde{x}^{2/3})\,, \tag{20}$$

and this can also be obtained directly from the reference medium group velocity surface as in equation (15).

The P-wave traveltime series is given by (Alkhalifah and Tsvankin 1995)

$$t^2(\tilde{x}) = t_{P0}^2(1+\tilde{x}_p^2 - 2\eta\tilde{x}_p^4 + ...)\,, \tag{21}$$

where the P-wave normalized offset $\tilde{x}_p = x / (t_{P0} v_{Pn})$. By the comparison of equations (18) and (21), they are identical in terms of the first and second terms coefficients with corresponding parameters, and the third term coefficient is negative in P-wave traveltime equation (-2η) but positive in S-wave traveltime equation ($2\eta/3$). So if the zero offset traveltime and NMO velocity are fixed, increasing η induces increase for the S-wave traveltime but decrease for the P-wave traveltime (Fig. 4b).

The S-wave traveltime derivatives are not defined at zero offset,

$$\left.\frac{d^n t}{dx^n}\right|_{x=0} = \pm\infty,\ n = 1,2,...\,, \tag{22}$$

which implies that there is a cusp at this position (Fig. 4c) and corresponds to the group velocity surface at the vertical direction.

For a multi-layered model with parameters shown in Table 2, we plot the once reflected S-wave traveltime curves shown as Fig. 5a. Note that there are not any events crossing even at the large offset. It indicates the S-wave reflected from deeper interface always arrives later than that reflected from shallower interface, no matter the deeper layers have larger or smaller velocities. We illustrate this phenomenon in terms of the slowness surface. Since the horizontal slowness is preserved for incident and reflected waves, the effective slowness surface can be defined as

$$q(p)_{eff} = \frac{\sum_{i=1}^{n} q_i(p) z_i}{\sum_{i=1}^{n} z_i}, \tag{23}$$

where i is the layer index, z_i and $q_i(p)$ are respectively the thickness and slowness surface equation in layer i. Taking equation (23) in equation (17), we can estimate the traveltime and offset for multi-layered models with the effective slowness surface. Thus, the P-wave moveout slope at large offset is determined by the upper limit of the effective horizontal slowness, and the S-wave moveout slope at large offset is determined by the lower limit of the effective horizontal slowness. The effective horizontal slowness range is determined by the intersection of the individual horizontal slowness range in each layer. For simplicity, we use a two-layered model for illustration. Figure 5b shows the typical slowness surfaces for P- and S-waves in layer 1 (blue curves), layer 2 (orange curves) and their effective counterparts (red curves). At large offset, the effective horizontal slowness is

$$p_{eff}^{P} \le \min\{p_1^{P}, p_2^{P}\} \tag{24}$$

for P-wave and

$$p_{eff}^{S} \ge \max\{p_1^{S}, p_2^{S}\} \tag{25}$$

for S-wave, where p_1^P and p_2^P are respectively the upper limits for P-wave horizontal slowness range (equation (3)) in layers 1 and 2, and p_1^S and p_2^S are respectively the lower limits for S-wave horizontal slowness range (equation (12)) in layers 1 and 2. Equations (24) and (25) can be extended to arbitrary number of acoustic VTI layers at large offset as follows,

$$p_{eff}^P \le \min\{p_i^P\} \tag{26}$$

for P-wave and

$$p_{eff}^S \ge \max\{p_i^S\} \tag{27}$$

for S-wave, where $i = 1, 2, ..., n$ and n is the layers number. The horizontal slowness represents the slope of the traveltime versus offset. Thus, S-wave in acoustic VTI medium avoids the intractable events crossing at the large offset, and this benefits the AVO analysis, velocity analysis and so on.

Dix-type equations

For S-wave in multi-layered acoustic VTI media, the Dix-type equations are defined by (Appendix C)

$$t_{S0}^{\Sigma} = \sum_j t_{S0,j} \qquad \frac{t_{S0}^{\Sigma}}{(V_{Sn}^{\Sigma})^2} = \sum_j \frac{t_{S0,j}}{V_{Sn,j}^2}, \qquad \frac{t_{S0}^{\Sigma}(3+8\eta_S^{\Sigma})}{(V_{Sn}^{\Sigma})^4} = \sum_j \frac{t_{S0,j}(3+8\eta_j)}{V_{Sn,j}^4}, \tag{28}$$

where t_{S0}^{Σ}, V_{Sn}^{Σ} and η_S^{Σ} are respectively the S-wave effective zero offset traveltime, NMO velocity and anellipticity, and the effective vertical group velocity $V_{S0}^{\Sigma} = (\sum_j t_{S0,j} V_{S0,j}) / t_{S0}^{\Sigma}$. The subscript j corresponds to layer number. It is noted that the P-wave effective NMO velocity squared $(V_{Pn}^{\Sigma})^2$ is an arithmetic mean of the individual $V_{Pn,j}^2$ in each layer with the zero offset interval traveltime being the weight coefficient (equation C11), while the S-wave effective

NMO velocity squared $(V_{Sn}^{\Sigma})^2$ is a result of the harmonic mean of the individual $V_{Sn,j}^2$ in each layer with the weight coefficient being $t_{S0,j}$.

In a homogeneous VTI medium, the P-wave parameters (v_{P0}, v_{Pn}, η) are related to the S-wave parameters (V_{S0}, V_{Sn} (or V_{SX}), η) by equations (10) and (19). However, in equation (28) the S-wave effective kinematical parameters are differently defined from those for P-wave (Alkhalifah 1997; Appendix C). To illustrate that, we use a two-layered model with parameters listed in Table 3 to test the validity of equations (10) and (19) for multi-layered acoustic VTI medium. The two acoustic layers have the same v_{P0} and v_{Pn} but different values for η. Four sets of parameters are calculated as the function of the layer 2 volume fraction (Fig. 6). $V_{P0}^{\Sigma(P)}$, $V_{Pn}^{\Sigma(P)}$ and η_P^{Σ} are respectively the P-wave effective vertical velocity, NMO velocity and anellipticity of the two-layered model calculated by equation (C11). $V_{S0}^{\Sigma(P)}$ and $V_{Sn}^{\Sigma(P)}$ are the S-wave effective vertical group velocity and NMO velocity, and the superscript "*P*" indicates that they are calculated from $V_{P0}^{\Sigma(P)}$, $V_{Pn}^{\Sigma(P)}$ and η_P^{Σ} by equations (10) and (19). $V_{S0}^{\Sigma(S)}$, $V_{Sn}^{\Sigma(S)}$ and η_S^{Σ} are respectively the S-wave effective vertical group velocity, NMO velocity and anellipticity of the two-layered model calculated by equation (28). $V_{P0}^{\Sigma(S)}$ and $V_{Pn}^{\Sigma(S)}$ are the P-wave effective vertical velocity and NMO velocity, and the superscript "S" means that they are calculated from $V_{S0}^{\Sigma(S)}$, $V_{Sn}^{\Sigma(S)}$ and η_S^{Σ} by equations (10) and (19).

For P-wave,

$$V_{P0}^{\Sigma(P)} \geq V_{P0}^{\Sigma(S)} \text{ and } V_{Pn}^{\Sigma(P)} \geq V_{Pn}^{\Sigma(S)}. \tag{29}$$

For S-wave,

$$V_{S0}^{\Sigma(P)} \geq V_{S0}^{\Sigma(S)} \text{ and } V_{Sn}^{\Sigma(P)} \geq V_{Sn}^{\Sigma(S)}. \tag{30}$$

The value of η_P^{Σ} is bounded by the values of η in each layer, while the η_S^{Σ} is more complex and can exceed the maximum value of η in each layer (Fig. 6c). Therefore, equations (10) and (19) are not valid for effective parameters in multi-layered acoustic VTI medium, and the two sets of parameters characterize different effective media corresponding to P- and S-waves. It also means that applying Dix-type equations (in P- and S-waves versions) results in different effective media.

Relative geometrical spreading

Estimating the relative geometrical spreading is important for the true amplitude processing (Cerveny 2005; Stovas and Ursin 2009). For the pure mode wave, the relative geometrical spreading equation for a VTI medium is given by (Ursin and Hokstad 2003)

$$L = L_n \Omega, \tag{31}$$

where the radiation pattern

$$\Omega = \cos\varphi, \tag{32}$$

and the geometrical spreading factor L_n is given by

$$L_n = \left| \frac{x}{p} \frac{dx}{dp} \right|^{1/2}. \tag{33}$$

Expanding L_n in series with respect to normalized offset gives the geometrical spreading factor for S-wave (Appendix C),

$$L_n = t_{S0} V_{Sn}^2 [\sqrt{3}\tilde{x}^{4/3} - \frac{\eta(3+4\eta)\tilde{x}^{8/3}}{3^{4/3}} + ...]. \tag{34}$$

One can see that at zero offset, $L_\eta = 0$. Figure 7 shows the P- and S-waves relative geometrical spreading for the medium with parameters in Table 1. The relative geometrical spreading functions increase with offset for both P- and S-waves. Note the intercept of S-wave relative geometrical spreading function is zero, and it indicates a cusp point at zero offset.

For a homogeneous acoustic VTI medium, the S-wave relative geometrical spreading factor at the infinite offset limit goes to infinity, although there is a cusp point at the horizontal symmetry axis (Appendix C). For S-wave in multi-layered acoustic VTI medium, the group angle φ in equation (32) corresponds to that in the top layer at the source and receiver points, and t_{S0}, V_{Sn} and η in equation (34) are replaced by the effective values in equation (28).

Conclusions

The acoustic anisotropic medium can be practical from the upscaling point of view, and this case can make η a large value and even infinite (Appendix D). We show that the P- and S-waves are defined by the same slowness surface equation in acoustic VTI medium having the different horizontal slowness ranges, and this practically avoids the mode conversion for reflected/transmitted waves at the interface between two acoustic VTI media. From the branch of the slowness surface corresponding to S-wave, the new parameters are defined from two asymptotes. Revising the slowness surface equation by newly defined parameters, the shape of the S-wave group velocity surface is estimated to be quasi-astroid shaped. The traveltime equation is derived, together with the Dix-type equations valid for S-wave in multi-layered acoustic VTI model. The traveltime derivatives are not defined at zero offset, which represents a cusp point. By a two-layered acoustic VTI model, we demonstrate that the once reflected events for S-wave do not cross at large offset. The relative geometrical spreading equation is also derived, and the cusp point at zero offset induces the S-wave relative geometrical spreading to be zero.

Acknowledgements

We would like to acknowledge the ROSE project and the China Scholarship Council (CSC) for financial support.

REFERENCES

Alkhalifah T. 1997. Velocity analysis using nonhyperbolic moveout in transversely isotropic media. *Geophysics* **62**, 1839-1854.

Alkhalifah T. 1998. Acoustic approximations for processing in transversely isotropic media. *Geophysics* **63**, 623-631.

Alkhalifah T. 2000. An acoustic wave equation for anisotropic media. *Geophysics* **65**, 1239-1250.

Alkhalifah T. and Tsvankin I. 1995. Velocity analysis for transversely isotropic media. *Geophysics* **60**, 1550-1566.

Backus G. E. 1962. Long-wave elastic anisotropy produced by horizontal layering. *Journal of Geophysical Research* **67**, 4427-4440.

Chandrasekhar S. 1992. *Liquid crystals*. Cambridge University Press.

Cerveny V. 2005. *Seismic ray theory*. Cambridge University Press.

Grechka V., Tsvankin I. and Cohen J. K. 1999. Generalized Dix equation and analytic treatment of normal‐moveout velocity for anisotropic media. *Geophysical Prospecting*, **47**(2), 117-148.

Grechka V., Zhang L. and Rector III J. W. 2004. Shear waves in acoustic anisotropic media. *Geophysics* **69**, 576-582.

Han Q. and Wu R. S. 2005. A one-way dual-domain propagator for scalar qP-waves in VTI media. *Geophysics* **70**(2), D9-D17.

Hestholm S. 2009. Acoustic VTI modeling using high-order finite differences. *Geophysics* **74**(5), T67-T73.

Roganov Y. and Stovas A. 2010. On shear-wave triplications in a multilayered transeversely isotropic medium with vertical symmetry axis. *Geophysical Prospecting* **58**(4), 549-559.

Schoenberg M. and Muir F. 1989. A calculus for finely layered anisotropic media. *Geophysics*, **54**, 581–589.

Stovas A. and Ursin B. 2009. Improved geometric-spreading approximation in layered transversely isotropic media. *Geophysics* **74**(5), D85-D95.

Stovas A. and Fomel S. 2012. Generalized nonelliptic moveout approximation in τ-p domain. *Geophysics* **77**, U23-U30.

Thomsen L. 1986. Weak elastic anisotropy. *Geophysics* **51**, 1954-1966.

Thomsen L. and Dellinger J. 2003. On shear-wave triplication in transversely isotropic media. *Journal of Applied Geophysics*, **54**(3), 289-296.

Tsvankin I. 2001. *Seismic signatures and analysis of reflection data in anisotropic media*. Elsevier Science.

Tsvankin I. and Thomsen L. 1994. Nonhyperbolic reflection moveout in anisotropic media. *Geophysics* **59**, 1290-1304.

Ursin B. and Hokstad K. 2003. Geometrical spreading in a layered transversely isotropic medium with vertical symmetry axis. *Geophysics* **68**, 2082-2091.

Zhang L., Rector III J. W. and Hoversten G. M. 2003. An acoustic wave equation for modeling in tilted TI media. 73rd SEG meeting, Dallas, USA, Expanded Abstracts, 153–156.

Zhou H., Zhang G. and Bloor R. 2006. An anisotropic acoustic wave equation for VTI media. 68th EAGE meeting, Vienna, Austria, Extended Abstracts, H033.

Appendix A

The P- and S-wave slowness surface equation in acoustic VTI media

The Christoffel equation for VTI media is given by (Tsvankin, 2001)

$$\begin{bmatrix} c_{11}\sin^2\theta + c_{55}\cos^2\theta - \rho v^2 & 0 & (c_{13}+c_{55})\sin\theta\cos\theta \\ 0 & c_{66}\sin^2\theta + c_{55}\cos^2\theta - \rho v^2 & 0 \\ (c_{13}+c_{55})\sin\theta\cos\theta & 0 & c_{55}\sin^2\theta + c_{33}\cos^2\theta - \rho v^2 \end{bmatrix} \begin{bmatrix} U_1 \\ U_2 \\ U_3 \end{bmatrix} = 0, \tag{A1}$$

where c_{11}, c_{13}, c_{33}, c_{55} and c_{66} are the five non-zero stiffness coefficients for VTI media, U_1, U_2 and U_3 are polarization vectors, θ is the phase angle taken from the vertical symmetry axis, ρ is the density and v is the wave phase velocity. For the coupled qP- and qSV-waves polarized in the vertical symmetry plane, their phase velocities and polarization vectors are determined by

$$\begin{bmatrix} c_{11}\sin^2\theta + c_{55}\cos^2\theta - \rho v^2 & (c_{13}+c_{55})\sin\theta\cos\theta \\ (c_{13}+c_{55})\sin\theta\cos\theta & c_{55}\sin^2\theta + c_{33}\cos^2\theta - \rho v^2 \end{bmatrix} \begin{bmatrix} U_1 \\ U_2 \end{bmatrix} = 0. \tag{A2}$$

The qP- and qSV-wave phase velocities can be obtained by solving

$$\begin{vmatrix} c_{11}\sin^2\theta + c_{55}\cos^2\theta - \rho v^2 & (c_{13}+c_{55})\sin\theta\cos\theta \\ (c_{13}+c_{55})\sin\theta\cos\theta & c_{55}\sin^2\theta + c_{33}\cos^2\theta - \rho v^2 \end{vmatrix} = 0, \tag{A3}$$

and the solutions can be written as

$$v(\theta)^2 = \frac{c_{55} + c_{33}\cos^2\theta + c_{11}\sin^2\theta \pm \sqrt{[(c_{55}-c_{33})\cos^2\theta + (c_{11}-c_{55})\sin^2\theta]^2 + (c_{13}+c_{55})^2\sin^2 2\theta}}{2\rho}, \tag{A4}$$

where positive and negative signs correspond to qP- and qSV-waves, respectively. Their polarization angle α_P and α_{SV} taken from the vertical axis are given by

$$\begin{aligned}\alpha_P &= -\arctan\frac{(c_{13}+c_{55})\sin\theta\cos\theta}{c_{11}\sin^2\theta + c_{55}\cos^2\theta - \rho v_P^2},\\ \alpha_{SV} &= \arctan\frac{c_{55}\sin^2\theta + c_{33}\cos^2\theta - \rho v_{SV}^2}{(c_{13}+c_{55})\sin\theta\cos\theta}.\end{aligned} \tag{A5}$$

The horizontal slowness p and vertical slowness q can be obtained from phase velocity as follows,

$$p = \sin\theta / v(\theta) \text{ and } q = \cos\theta / v(\theta). \tag{A6}$$

Substituting equation (A6) into equation (A4) gives the slowness surface as

$$(c_{11}+c_{55})p^2 + (c_{33}+c_{55})q^2 \pm \sqrt{2(c_{13}+c_{55})^2 p^2 q^2 + [(c_{11}-c_{55})p^2 + (c_{55}-c_{33})q^2]^2} = 2\rho. \tag{A7}$$

One can note that the qP- and qSV-waves slowness surfaces are defined by the normalized parameters: c_{11}/ρ, c_{13}/ρ, c_{33}/ρ and c_{55}/ρ. These four parameters can be rewritten by

$$\begin{aligned}c_{11}/\rho &= v_{Pn}^2(1+2\eta),\\ c_{33}/\rho &= v_{P0}^2,\\ c_{13}/\rho &= v_{S0}^2\left(\sqrt{(v_{P0}^2/v_{S0}^2 - 1)(v_{Pn}^2/v_{S0}^2 - 1)} - 1\right),\\ c_{55}/\rho &= v_{S0}^2,\end{aligned} \tag{A8}$$

where v_{P0} and v_{S0} are respectively the P- and S-waves vertical phase velocities, $\eta = (\varepsilon - \delta)/(1+2\delta)$ is the anelliptic parameter (Alkhalifah and Tsvankin 1995), $v_{Pn}^2 = v_{P0}^2(1+2\delta)$ is the P-wave NMO velocity, ε and δ are the Thomsen parameters (Thomsen 1986). Substituting equation (A8) into equation (A7) gives the qP- and qSV-waves slowness surface equations as follows,

$$aq^4 + bq^2 + c = 0, \tag{A9}$$

where

$$\begin{aligned} a &= v_{S0}^2 v_{P0}^2, \\ b &= v_{S0}^2[p^2(v_{Pn}^2 + v_{P0}^2) - 1] + v_{P0}^2(2\eta v_{Pn}^2 p^2 - 1), \\ c &= (p^2 v_{S0}^2 - 1)[(1+2\eta)v_{Pn}^2 p^2 - 1]. \end{aligned} \tag{A10}$$

In the following, we consider the two cases of elastic VTI media ($v_{S0} \neq 0$) and acoustic VTI media ($v_{S0} \neq 0$).

For elastic VTI media with $v_{S0} \neq 0$ (i.e., $a \neq 0$), the vertical slowness q for qP- and qSV-waves as a function of horizontal slowness p is given by

$$q = \sqrt{\frac{-2c}{b \pm \sqrt{b^2 - 4ac}}}, \tag{A11}$$

where positive and negative signs respectively correspond to qSV- and qP-waves, and this can be verified by the corresponding vertical slowness values when $p = 0$ in the symmetry axis direction. Since parameter a in equation (A9) is positive, different signs of the parameters b and c lead to various solutions of q^2 in equation (A9). Specially, there are six cases as listed in Table A1. The sign of the parameter b can be written as

$$\begin{cases} b > 0, & \text{if } p > p_b; \\ b = 0, & \text{if } p = p_b; \\ b < 0, & \text{if } 0 < p < p_b \text{ or } \eta < -v_{S0}^2(v_{P0}^2 + v_{Pn}^2)/(2v_{P0}^2 v_{Pn}^2), \end{cases} \tag{A12}$$

where

$$p_b = \frac{1}{v_{S0}} \sqrt{\frac{\frac{v_{P0}^2}{v_{S0}^2} + 1}{\frac{v_{Pn}^2}{v_{S0}^2} + \frac{v_{P0}^2}{v_{S0}^2}\left(1 + \frac{2\eta v_{Pn}^2}{v_{S0}^2}\right)}} . \tag{A13}$$

The sign of the parameter c is given by

$$\begin{cases} c > 0, & \text{if } p < 1/v_{Ph} \text{ or } p > 1/v_{S0}, \\ c = 0, & \text{if } p = 1/v_{Ph} \text{ or } p = 1/v_{S0}, \\ c < 0, & \text{if } 1/v_{Ph} < p < 1/v_{S0}, \end{cases} \tag{A14}$$

where $v_{Ph} = v_{Pn}\sqrt{1+2\eta}$ is the P-wave horizontal velocity (Alkhalifah and Tsvankin 1995)).

Case 1 in Table A1 gives two solutions correspond to the evanescent waves, and it is ignored in this paper. Only case 3 with non-negative parameter c gives the vertical slowness solution for P-wave, and the P-wave horizontal slowness range is given by

$$0 \le p \le 1/(v_{Pn}\sqrt{1+2\eta}) . \tag{A15}$$

The qSV-wave emerges in cases 2-6. Cases 2, 3, and 6 individually gives one solution for qSV-wave, and the corresponding horizontal slowness has a range given by

$$0 \le p \le 1/v_{S0} . \tag{A16}$$

The cases 4 and 5 individually gives two qSV-wave vertical slowness values for a certain horizontal slowness. In case 4, two different qSV-wave vertical slowness values indicate the presence of horizontal triplication (Thomsen and Dellinger 2003), and the parameter p_b^* in Table A1 can be obtained by solving

$$(b^2 - 4ac)\Big|_{p=p_b^*} = 0 \text{ and } p_b^* > 1/v_{S0} , \tag{A17}$$

where parameters *a*, *b*, *c* are given in equation (A10) . Since case 4 requires $b < 0$ and $c \geq 0$, the criteria can be deduced from equations (A12) and (A14) as follows,

$$p_b > \frac{1}{v_{S0}} \text{ or } \eta < \frac{-v_{S0}^2(v_{P0}^2 + v_{Pn}^2)}{2v_{P0}^2 v_{Pn}^2}. \tag{A18}$$

The case 5 corresponds to the incipient qSV-wave horizontal triplication. Since case 5 requires $b = 0$ and $c = 0$, the criteria can be deduced from equations (A12) and (A14) as follows,

$$p_b^* = p_b = \frac{1}{v_{S0}}. \tag{A19}$$

Taking into account of equations (A13), (A18) and (A19), the criteria for existing qSV-wave horizontal triplication (including incipient triplication) is given by

$$\eta \leq \frac{v_{S0}^2(v_{S0}^2 - v_{Pn}^2)}{2v_{P0}^2 v_{Pn}^2}. \tag{A20}$$

Therefore, if the model parameters satisfy equation (A20), there is horizontal qSV-wave triplication, and the corresponding horizontal slowness has a range given by

$$0 \leq p \leq p_b^*. \tag{A21}$$

For acoustic VTI media with $v_{S0} = 0$ (i.e., $a = 0$), equation (A9) reduces to

$$b_s q^2 + c_s = 0, \tag{A22}$$

where

$$\begin{aligned} b_s &= v_{P0}^2(2\eta v_{Pn}^2 p^2 - 1), \\ c_s &= 1 - (1 + 2\eta) v_{Pn}^2 p^2, \end{aligned} \tag{A23}$$

and the vertical slowness q for P- and S-waves as a function of horizontal slowness p is given by

$$q = \sqrt{\frac{-c_s}{b_s}}\,. \tag{A24}$$

When the horizontal slowness surface satisfy

$$\frac{1}{v_{Pn}\sqrt{1+2\eta}} < p < \frac{1}{v_{Pn}\sqrt{2\eta}}\,, \tag{A25}$$

the radical term in equation (A24) is negative and lead to evanescent waves.

Since we ignore the evanescent waves, the term $c_s / b_s \le 0$. Therefore, the range of the horizontal slowness surface is

$$0 \le p \le \frac{1}{v_{Pn}\sqrt{1+2\eta}} \tag{A26}$$

for P-wave and

$$\frac{1}{v_{Pn}\sqrt{2\eta}} \le p \le +\infty \tag{A27}$$

for S-wave. One can note the infinite S-wave horizontal slowness leads to the horizontal asymptote given by

$$p = +\infty,\ q = \frac{1}{v_{P0}}\sqrt{\frac{1+2\eta}{2\eta}}\,. \tag{A28}$$

When the S-wave horizontal slowness reaches its lower limit $1/(v_{Pn}\sqrt{2\eta})$, the vertical asymptote can be obtained as follows,

$$p = \frac{1}{v_{Pn}\sqrt{2\eta}},\ q = +\infty . \tag{A29}$$

The P- and S-wave polarization angles in equation (A5) reduce to

$$\begin{aligned}
\alpha_P &= \arctan \frac{v_{P0}v_{Pn}\sin 2\theta}{v_{P0}^2\cos^2\theta - v_{Pn}^2\sin^2\theta - 2\eta v_{Pn}^2\sin^2\theta + \sqrt{(v_{P0}^2\cos^2\theta - (1+2\eta)v_{Pn}^2\sin^2\theta)^2 + v_{P0}^2v_{Pn}^2\sin^2 2\theta}}, \\
\alpha_S &= \arctan \frac{v_{P0}^2\cos^2\theta - v_{Pn}^2\sin^2\theta - 2\eta v_{Pn}^2\sin^2\theta + \sqrt{(v_{P0}^2\cos^2\theta - (1+2\eta)v_{Pn}^2\sin^2\theta)^2 + v_{P0}^2v_{Pn}^2\sin^2 2\theta}}{v_{P0}v_{Pn}\sin 2\theta},
\end{aligned} \tag{A30}$$

where α_P and α_S are the P- and S-wave polarization angles taken from the vertical axis.

Appendix B

The quasi-astroid shaped S-wave group velocity surface

The group velocity vertical and horizontal components V_{GZ} and V_{GX} are can be obtained from the slowness surfaces as follows (Grechka, Tsvankin and Cohen 1999),

$$V_{GZ} = \frac{1}{q - pdq/qp} \quad \text{and} \quad V_{GX} = \frac{-dq/dp}{q - pdq/qp}, \tag{B1}$$

where p and q are respectively the horizontal and vertical slowness. V_{GZ} and V_{GX} are also defined as the group velocity projections given by

$$V_{GX} = V_G \sin\varphi \text{ and } V_{GZ} = V_G \cos\varphi, \tag{B2}$$

where V_G is the group velocity and φ is the group angle taken from the vertical direction. We can obtain the velocity V_G and group angle φ as follows,

$$V_G = \frac{\sqrt{1+(dq/dp)^2}}{q - pdq/qp} \quad \text{and} \quad \tan\varphi = -\frac{dq}{dp}. \tag{B3}$$

Taking equation (5) into equation (B3) leads to the P- and S-wave group velocities and group angles as the functions of horizontal slowness in acoustic VTI media,

$$V_G(p)=\frac{\sqrt{p^2v_{Pn}^4+v_{P0}^2(2\eta p^2v_{Pn}^2-1)^3[(1+2\eta)p^2v_{Pn}^2-1]}}{(2\eta p^2v_{Pn}^2-1)^2+2\eta p^4v_{Pn}^4},$$
$$\varphi(p)=\arctan\frac{pv_{Pn}^2}{v_{P0}\sqrt{(1-2p^2v_{Pn}^2\eta)^3[1-p^2v_{Pn}^2(1+2\eta)]}}, \tag{B4}$$

where P- and S-waves have distinctive slowness ranges given by equations (3) and (6), respectively.

Taking the lower limit for S-wave horizontal slowness $p=1/(v_{Pn}\sqrt{2\eta})$ into equation (B4) leads to $\varphi=\pi/2$, and the S-wave horizontal group velocity V_{SX} is given by

$$V_{SX}=v_{Pn}\sqrt{2\eta}\,. \tag{B5}$$

The upper limit for S-wave horizontal slowness $p=+\infty$ gives $\varphi=0$, and the S-wave vertical group velocity V_{S0} is given by

$$V_{S0}=v_{P0}\sqrt{\frac{2\eta}{1+2\eta}}\,. \tag{B6}$$

The new S-wave parameters are defined as V_{S0}, V_{SX} and η. For S-wave in acoustic VTI medium, substituting equation (11) into equation (B3) gives the parametric equations for group velocity $V_G(p)$ and group angle $\varphi(p)$. The ray velocity projections as the functions of horizontal slowness can be obtained by equation (B2). For the reference medium ($\eta=0$), equation (11) reduces to equation (13). Taking into account of the group velocity projections in equation (B2), the group velocity surface for S-wave in a reference medium is defined by the astroid equation

$$\left(\frac{\sin\varphi}{V_{SX}}\right)^{2/3}+\left(\frac{\cos\varphi}{V_{S0}}\right)^{2/3}=\frac{1}{V_G^{2/3}}\,. \tag{B7}$$

The S-wave vertical slowness is a convex function of the horizontal slowness (Fig. 2). Analytically, taking the second order derivative of equation (11) gives

$$\frac{d^2q}{dp^2}=\frac{V_{SX}^2[3p^4V_{SX}^4+2\eta(3p^2V_{SX}^2+1)(p^2V_{SX}^2-1)]}{V_{S0}(p^2V_{SX}^2-1)^{5/2}[p^2V_{SX}^2(1+2\eta)-2\eta]^{3/2}\sqrt{(1+2\eta)}}\geq 0 \tag{B8}$$

for S-wave horizontal slowness range $V_{SX}^{-1} \le p \le +\infty$. Roganov and Stovas (2010) pointed out that the positive values of d^2q/dp^2 indicate the presence of triplication for the horizontal slowness p, and the zero values refer to the incipient triplication. Therefore, the S-wave corresponds to a branch in the triplication.

Appendix C

The traveltime and relative geometrical spreading equations

In an acoustic VTI medium, the source-receiver offset and traveltime are defined from the slowness surface as (Stovas and Fomel 2012)

$$\begin{aligned} x &= -V_{S0}t_{S0}\frac{dq}{dp}, \\ t &= qV_{S0}t_{S0} + px, \end{aligned} \tag{C1}$$

where the zero offset two-way traveltime $t_{S0} = 2z/V_{S0}$, and z is the thickness of the layer. The Taylor expansion of offset and traveltime at the infinite horizontal slowness gives the S-wave moveout in the slowness domain as follows,

$$\begin{aligned} x &= t_{S0}V_{Sn}\left(\frac{1}{V_{Sn}^3p^3} + \frac{3+8\eta}{2V_{Sn}^5p^5} + \ldots\right), \\ t &= t_{S0}\left(1 + \frac{3}{2V_{Sn}^2p^2} + \frac{15+40\eta}{8V_{Sn}^4p^4} + \ldots\right). \end{aligned} \tag{C2}$$

In order to get the direct moveout series in the offset domain, we first apply the series inversion for the offset x in equation (C2) and obtain

$$p = \frac{t_{S0}^{1/3}}{V_{Sn}^{2/3}x^{1/3}} + \frac{(3+8\eta)x^{1/3}}{6t_{S0}^{1/3}V_{Sn}^{4/3}} + \ldots . \tag{C3}$$

Then, substituting series (C3) into the traveltime t in equation (C2) results in the S-wave moveout series in offset domain given by

$$t^{2/3}(\tilde{x}) = t_{S0}^{2/3}(1+\tilde{x}^{2/3}+\frac{2}{3}\eta\tilde{x}^{4/3}+...), \tag{C4}$$

where the normalized offset $\tilde{x} = x/(t_{S0}V_{Sn})$. If $\eta = 0$, the traveltime equation reduces to

$$t^{2/3}(\tilde{x}) = t_{S0}^{2/3}(1+\tilde{x}^{2/3}), \tag{C5}$$

which can also be obtained directly from the reference medium group velocity surface equation (B7).

The S-wave geometrical spreading factor L_η can be computed from equation (33) by the substitution of equation for offset in equation (C2),

$$L_\eta = \frac{t_{S0}V_{Sn}^2\sqrt{3p^4V_{Sn}^4-4p^2V_{Sn}^2\eta-2\eta(1+2\eta)}}{(p^2V_{Sn}^2-2\eta)(p^2V_{Sn}^2-2\eta-1)^2}. \tag{C6}$$

Equation (C6) estimates the S-wave geometrical spreading in the slowness domain. Taking into account equation (C3), the relative geometrical spreading factor can be expanded into series about offset,

$$L_\eta = t_{S0}V_{Sn}^2[\sqrt{3}\tilde{x}^{4/3}-\frac{\eta(3+4\eta)\tilde{x}^{8/3}}{3^{4/3}}+...]. \tag{C7}$$

At zero offset, the relative geometrical spreading factor $L_\eta = 0$.

One can see that at the infinite offset, the relative geometrical spreading factor has the limit as

$$\lim_{pV_{Sn}\to\sqrt{1+2\eta}} L_\eta = \infty. \tag{C8}$$

So the S-wave relative geometrical spreading factor value increases with offset and goes to infinity at infinite offset limit.

For the multi-layered case, the effective kinematical parameters can be estimated from the effective slowness surface. Since the horizontal slowness is preserved for incident and reflected waves, the effective slowness surface can be defined as

$$q(p)_{eff} = \frac{\sum_{i=1}^{n} q_i(p) z_i}{\sum_{i=1}^{n} z_i}, \tag{C9}$$

where i is the layer index, z_i and $q_i(p)$ are respectively the thickness and slowness surface equation in layer i. For P-wave, the Dix-type equations can be derived from the averaging of the series coefficients for the Taylor expansion of equation (5) at $p = 0$,

$$q = \frac{1}{v_{P0}} - \frac{v_{Pn}^2 p^2}{2v_{P0}} - \frac{v_{Pn}^4 (1+8\eta) p^4}{8v_{P0}} + \ldots . \tag{C10}$$

That gives

$$\begin{aligned} t_{P0}^{\Sigma} &= \sum_j t_{P0,j}, \\ t_{P0}^{\Sigma} (V_{Pn}^{\Sigma})^2 &= \sum_j t_{P0,j} v_{Pn,j}^2, \\ t_{P0}^{\Sigma} (V_{Pn}^{\Sigma})^4 (1+8\eta_P^{\Sigma}) &= \sum_j t_{P0,j} v_{Pn,j}^4 (1+8\eta_j), \end{aligned} \tag{C11}$$

where t_{P0}^{Σ}, V_{Pn}^{Σ} and η_P^{Σ} are the P-wave effective zero offset traveltime, NMO velocity and anellipticity, and the effective vertical velocity $V_{P0}^{\Sigma} = (\sum_j t_{P0,j} v_{P0,j}) / t_{P0}^{\Sigma}$.

For S-wave, the similar procedure should also be applied for short offset. Thus, the Taylor expansion of equation (11) at infinite horizontal slowness gives

$$q = \frac{1}{V_{S0}} + \frac{1}{2V_{S0}V_{Sn}^2 p^2} + \frac{3+8\eta}{8V_{S0}V_{Sn}^4 p^4} + \dots . \tag{C12}$$

The S-wave Dix type equations have the form as

$$\begin{aligned} t_{S0}^{\Sigma} &= \sum_j t_{S0,j}, \\ \frac{t_{S0}^{\Sigma}}{(V_{Sn}^{\Sigma})^2} &= \sum_j \frac{t_{S0,j}}{V_{Sn,j}^2}, \\ \frac{t_{S0}^{\Sigma}(3+8\eta_S^{\Sigma})}{(V_{Sn}^{\Sigma})^4} &= \sum_j \frac{t_{S0,j}(3+8\eta_j)}{V_{Sn,j}^4}, \end{aligned} \tag{C13}$$

where V_{S0}^{Σ}, V_{Sn}^{Σ} and η_S^{Σ} are the S-wave effective zero offset traveltime, NMO velocity and anellipticity, and the S-wave effective vertical group velocity $V_{S0}^{\Sigma} = (\sum_j t_{S0,j} V_{S0,j}) / t_{S0}^{\Sigma}$. The comparison of Dix-type equations for P-wave (equation (C11)) and S-wave (equation (C13)) shows that the effective media defined by Dix-type equations for P- and S-waves are different.

Appendix D

The acoustic anisotropic media from the thin layering

This appendix has a brief view of the results in Grechka *et al*. (2004). According to the "long wave equivalent" medium theory (Backus 1962), a stack of thin isotropic or transversely isotropic layers can be replaced with an effective medium with parameters defined by

$$\begin{aligned} C_{11} &= \left\langle C_{11}^k - (C_{13}^k)^2 (C_{33}^k)^{-1} \right\rangle + \left\langle C_{13}^k (C_{33}^k)^{-1} \right\rangle^2 \left\langle (C_{33}^k)^{-1} \right\rangle^{-1}, \\ C_{33} &= \left\langle (C_{33}^k)^{-1} \right\rangle^{-1}, \\ C_{13} &= \left\langle C_{13}^k (C_{33}^k)^{-1} \right\rangle \left\langle (C_{33}^k)^{-1} \right\rangle^{-1}, \\ C_{44} &= \left\langle (C_{44}^k)^{-1} \right\rangle^{-1}, \\ C_{66} &= \left\langle C_{66}^k \right\rangle, \\ \rho &= \left\langle \rho^k \right\rangle, \end{aligned} \tag{D1}$$

where C_{ij}^k and ρ^k are the stiffness coefficient and density for layer k, and $\langle\ \rangle$ means arithmetic averaging with the layer thickness as a weight factor. If any layer has $C_{44}^k = 0$ (or $v_{S0}^k = 0$), corresponding to the fluid layer, the effective coefficient C_{44} in equation (D1) turns out to be zero, implying that the effective medium is an acoustic VTI medium (Grechka *et al.* 2004). Although the acoustic VTI was initially introduced as an artificial model (Alkhalifah 1998), one can see that this model can also be obtained from the physical principles. This practical acoustic VTI medium can be fully described with the vertical P-wave phase velocity v_{P0} and two Thomsen parameters ε, δ or their combination η (Alkhalifah 1995), defined as

$$
\begin{aligned}
v_{P0}^2 &= \frac{C_{33}}{\rho}, \\
\varepsilon &= \frac{C_{11} - C_{33}}{2C_{33}}, \\
\delta &= \frac{C_{13}^2 - C_{33}^2}{2C_{33}^2}, \\
\eta &= \frac{\varepsilon - \delta}{1 + 2\delta} = \frac{1}{2}\left(\frac{C_{11}C_{33}}{C_{13}^2} - 1\right).
\end{aligned}
\tag{D2}
$$

We notice the parameter δ is differently defined from the notional acoustic VTI case, where C_{44} is usually a non-zero value while the v_{S0} is artificially set to be zero ($v_{S0} \neq \sqrt{C_{44}/\rho}$). But for the finely layered case, both C_{44} and v_{S0} are physically zero, making the two sets of parameterization equivalent.

Using a binary medium composed of interlayering plane solid layers ($V_P = 3.00 km/s$, $V_S = 2.12 km/s$, $\rho = 2.00 g/cm^3$) and fluid layers ($V_{Pf} = 1.50 km/s$, $\rho_f = 1.00 g/cm^3$), we plot ε, δ and η as the function of fluid volume fraction ϕ (Fig. A1). One can see that ε and δ have different signs and strong magnitudes. In particular, at $\phi = 0$, $\delta = -0.5$ indicates the remaining slip at solid-fluid interface. The anellipticity coefficient η turns out to be infinite

when $\phi = 0$ (Fig. A1b), which is an extremely anisotropic case and induces the P-wave singularity (Grechka *et al*. 2004).

The medium parameters used to plot Fig. A1 are designed to make $\eta = \infty$ when $\phi = 0$. For the general case, when C_{13} in equation (D2) is zero, $\delta = -0.5$ and $\eta = \infty$. For a binary medium composed of finely interlayering plane solid isotropic layers and fluid layers, the C_{13} in equation (D1) is

$$C_{13} = \frac{V_{Pf}^2 \rho_f \rho [V_P^2 + 2V_S^2 (\phi - 1)]}{V_S^2 \rho \phi - V_{Pf}^2 \rho_f (\phi - 1)}, \tag{D3}$$

where the isotropic solid layer is defined by P-wave velocity V_P, S-wave velocity V_S and density ρ. The fluid layer is defined by P-wave velocity V_{Pf} and density ρ_f. ϕ is the fluid layer volume fraction.

If $\phi = 0$, as long as the solid layer parameters have the following relationship

$$V_P^2 = 2V_S^2, \tag{D4}$$

the binary medium would be extremely anisotropic ($\eta = \infty$).

Grechka *et al*. (2004) pointed out that the acoustic anisotropic media with lower symmetry than acoustic VTI can also be obtained from the upscaling point of view. Interestingly, the interlayering of triclinic layers and fluid layers induces the acoustic monoclinic by applying the averaging method proposed in Schoenberg and Muir (1989).

v_{P0} (km/s)	v_{Pn} (km/s)	η	V_{S0} (km/s)	V_{SX} (km/s)	V_{Sn} (km/s)	z (km)
2.00	2.20	0.50	1.40	2.20	3.11	1.00

Table 1 Parameters of a homogeneous acoustic VTI medium.

layer	z (km)	η	V_{S0} (km/s)	V_{Sn} (km/s)
1	0.30	1.92	1.40	4.8
2	0.40	2.53	1.63	5.4
3	0.70	4.06	1.85	7.2
4	0.60	5.31	1.68	7.8
5	0.50	3.42	1.60	5.8

Table 2 Parameters of a multi-layered acoustic VTI medium.

layer	v_{P0} (km/s)	v_{Pn} (km/s)	η	V_{S0} (km/s)	V_{Sn} (km/s)
1	2.00	2.20	0.10	0.82	1.08
2	2.00	2.20	0.40	1.34	2.64

Table 3 Parameters of a two-layered acoustic VTI medium.

Cases	Horizontal slowness	Parameters in equation (A11)		Slowness solution 1		Slowness solution 2	
		b	c	Vertical slowness	Wave type	Vertical slowness	Wave-type
Case 1	$p \in [0, +\infty)$	$b \geq 0$	$c > 0$	$q_1^2 < 0$	evanescent wave	$q_2^2 < 0$	evanescent wave
Case 2	$p \in (v_{Ph}^{-1}, v_{S0}^{-1})$	$(-\infty, +\infty)$	$c < 0$	$q_1^2 < 0$	evanescent wave	$q_2^2 > 0$	SV-wave
Case 3	$p \in [0, v_{Ph}^{-1}]$	$b < 0$	$c \geq 0$	$q_1^2 \geq 0$	P-wave	$q_2^2 > 0$	SV-wave
Case 4	$p \in [v_{S0}^{-1}, p_b^*)$, $p_b^* \leq p_b$	$b < 0$	$c \geq 0$	$q_1^2 > 0$	SV-wave	$q_2^2 > 0$	SV-wave
Case 5	$p = v_{S0}^{-1} = p_b^* = p_b$	$b = 0$	$c = 0$	$q_1^2 = 0$	SV-wave	$q_2^2 = 0$	SV-wave
Case 6	$p = v_{S0}^{-1}$	$b > 0$	$c = 0$	$q_1^2 < 0$	evanescent wave	$q_2^2 = 0$	SV-wave

Table A1 The six cases for the signs of parameters *b* and *c* in equation (A11), together with the equation solutions and corresponding wave types.

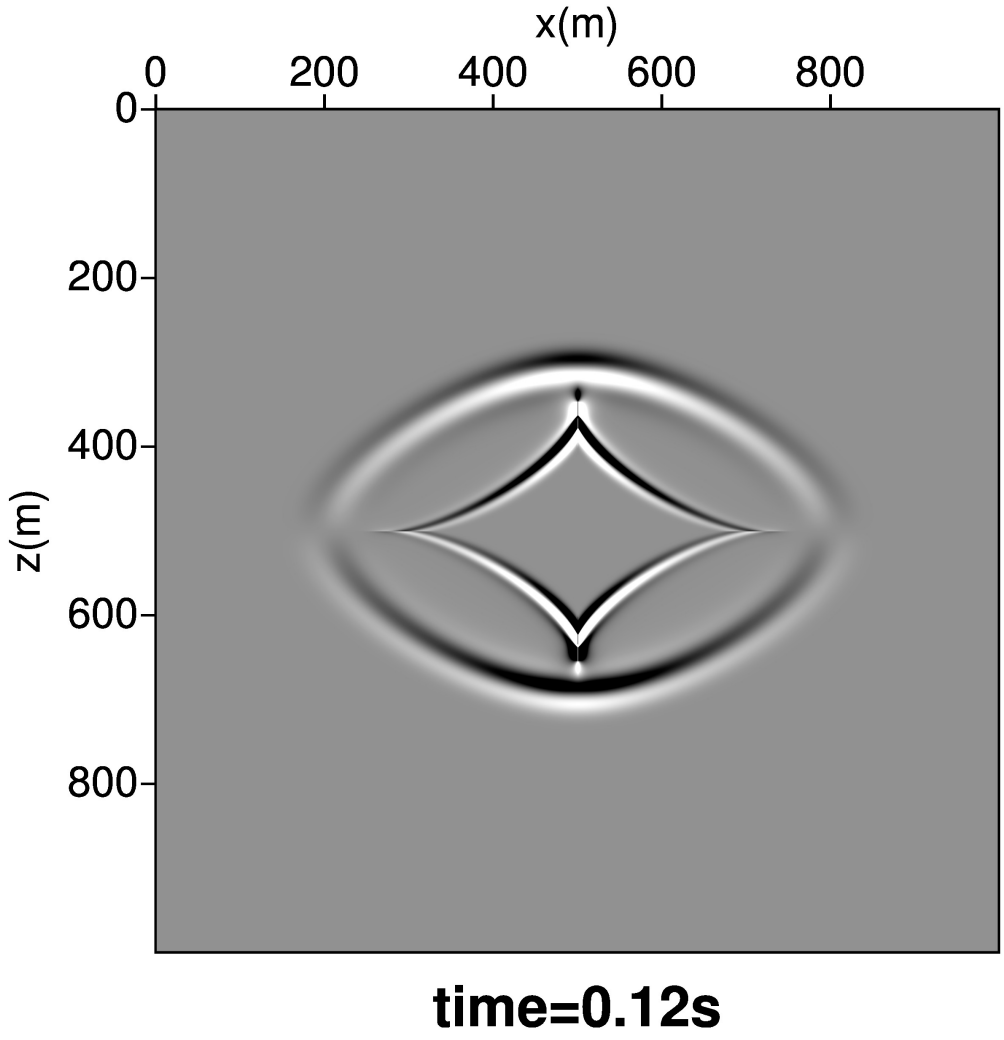

Figure 1 The wavefield snapshot for a homogeneous acoustic VTI medium. The exterior quasi-elliptical shaped wavefront is the P-wave and the interior quasi-astroid shaped wavefront corresponds to the S-wave.

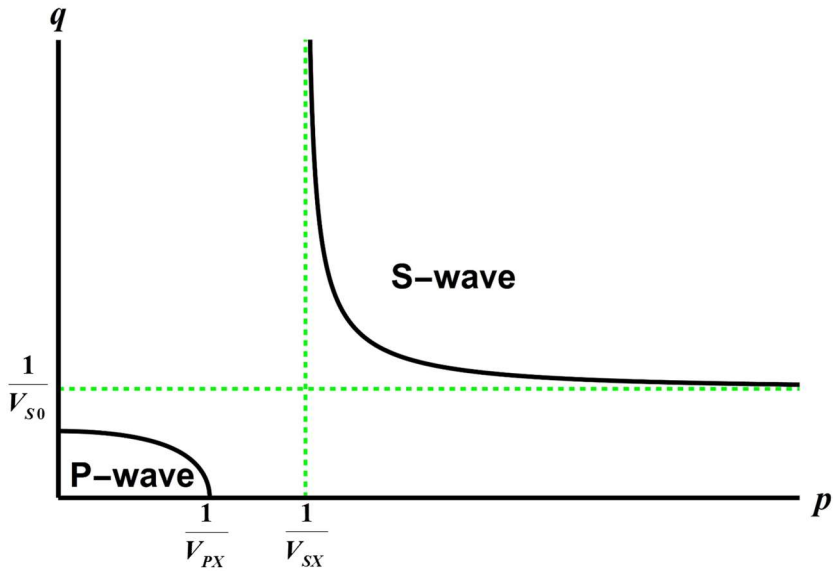

Figure 2 The sketch of the slowness surface of P- and S-waves in an acoustic VTI medium. V_{S0} is the S-wave group velocity in the vertical direction, and V_{PX} and V_{SX} are respectively P- and S-wave group velocities in the horizontal direction.

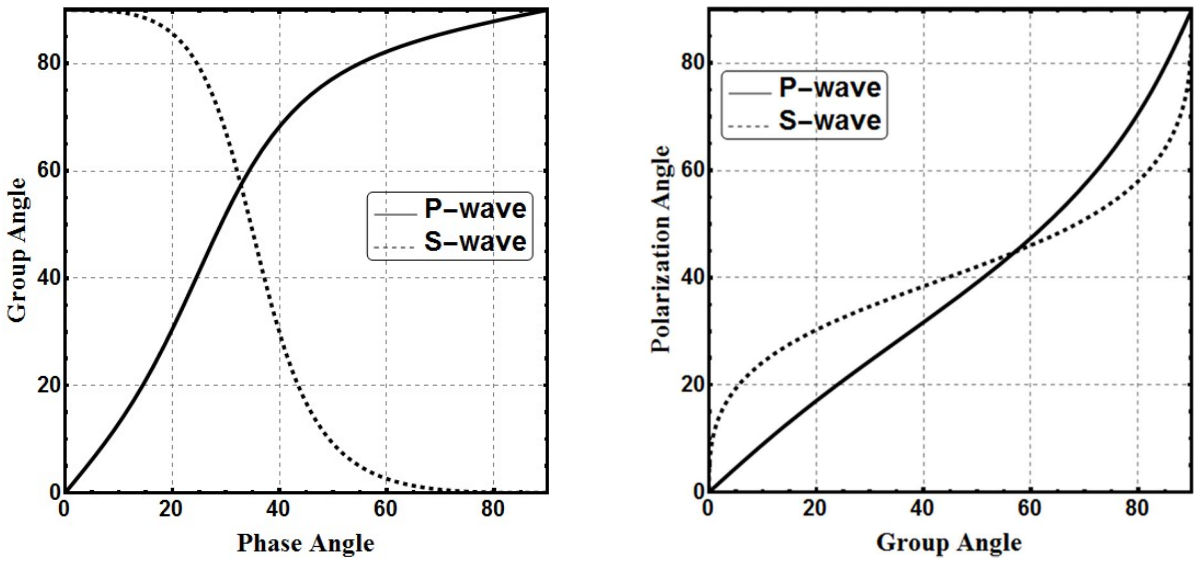

(a) (b)

Figure 3 The phase angle — group angle (a) and group angle — polarization angle (b) relationships for P- and S-waves in a homogeneous acoustic VTI medium. The model parameters are listed in Table 1.

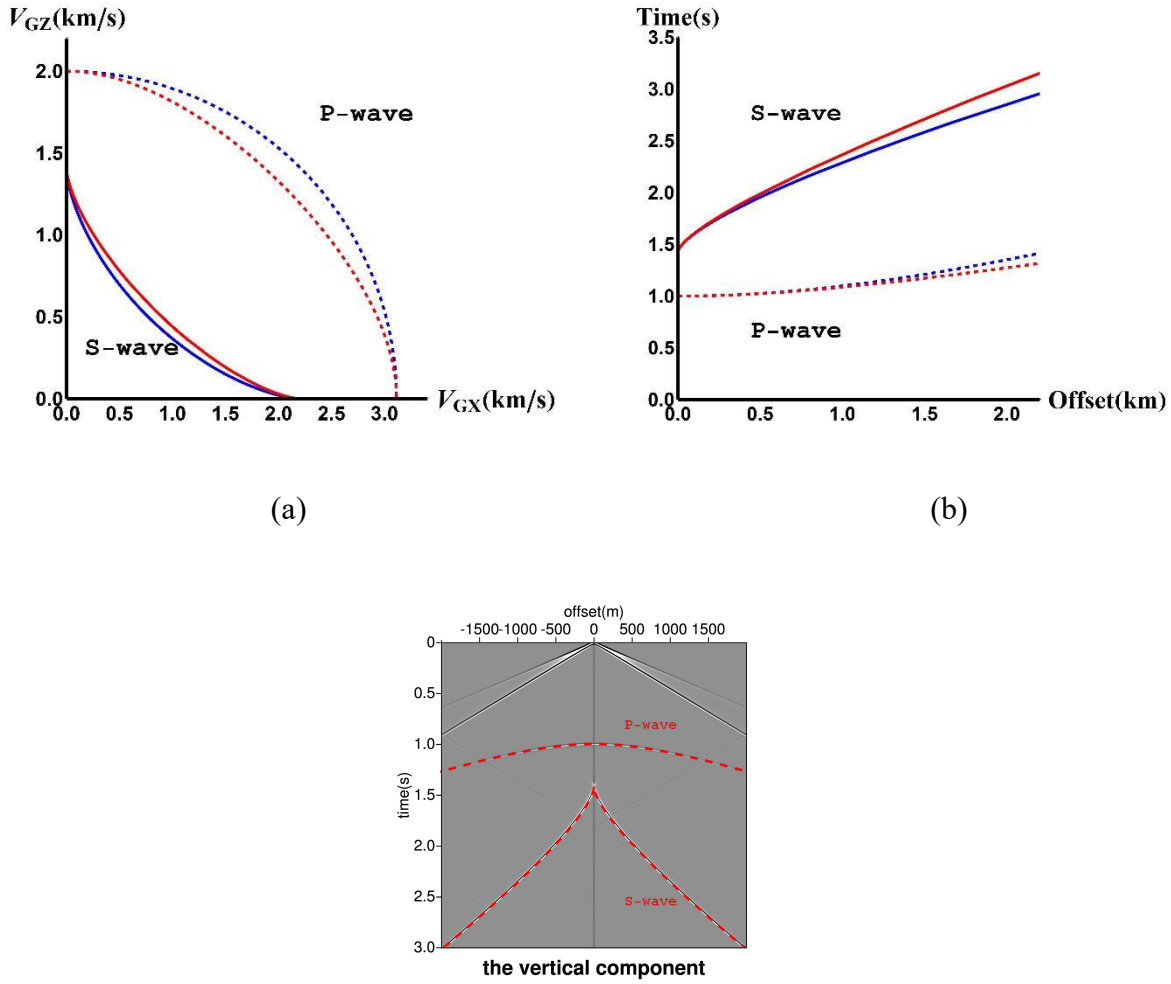

Figure 4 The group velocity surfaces (a) and traveltime curves (b) for P- (dashed lines) and S- (solid lines) waves in the acoustic VTI medium with parameters in Table 1 (red curves) and for the case with $\eta = 0$ (blue curves), together with the numerical modeling data (c) as a comparison for the analytical solution (equation 17) for the model with parameters listed in Table 1.

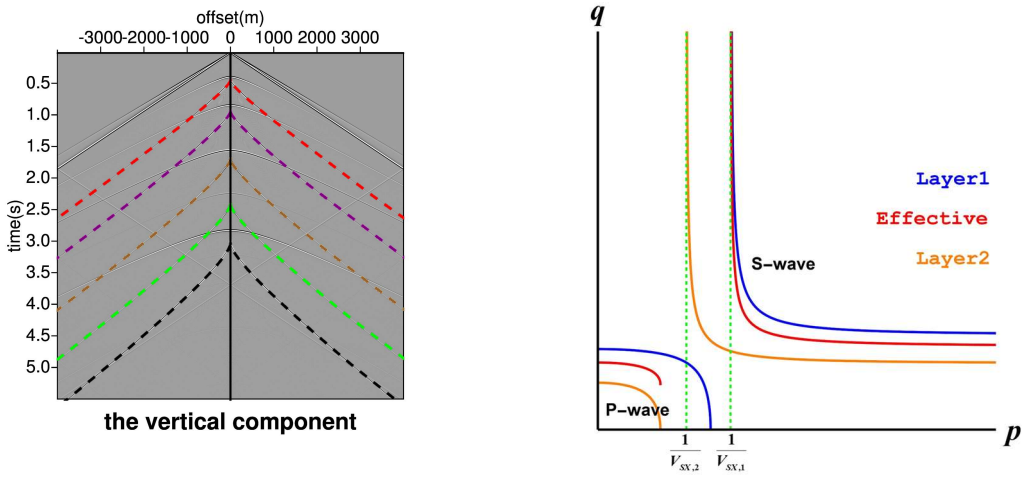

(a) (b)

Figure 5 (a) The traveltime (dashed curves) of once reflected S-wave from each layer bottom in a multi-layered acoustic VTI medium. Numerical modeling results are overlapped and the model parameters are shown in Table 2. (b) Typical slowness surfaces for a two-layered acoustic VTI model. $V_{PX,1}$ and $V_{PX,2}$ are respectively the S-wave horizontal group velocities in layer 1 and 2.

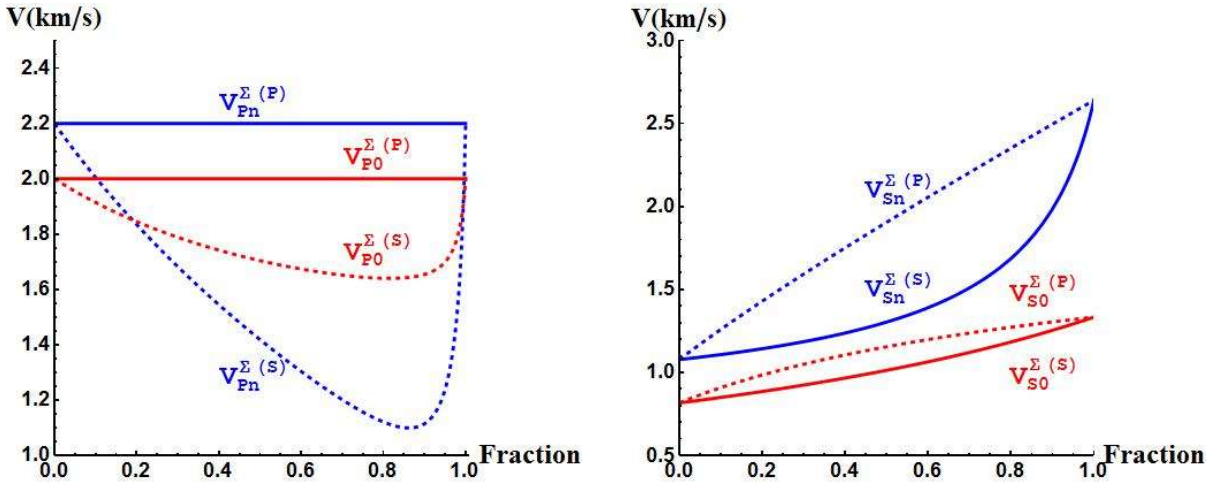

(a) (b)

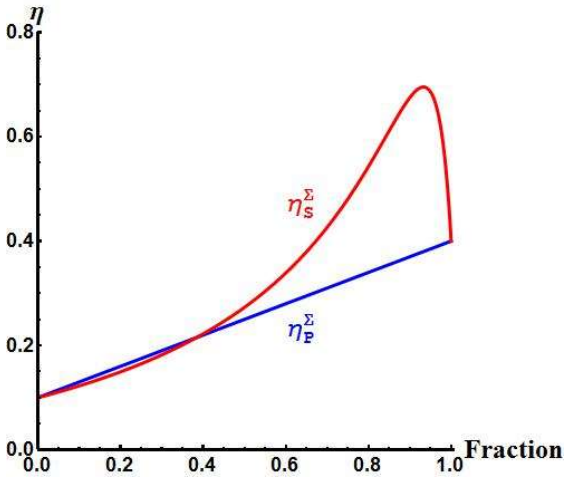

(c)

Figure 6 The kinematical parameters for P- and S-waves in a two-layered acoustic VTI model with parameters shown in Table 3. The P-wave effective kinematical parameters $V_{P0}^{\Sigma(P)}$, $V_{Pn}^{\Sigma(P)}$, η_P^{Σ} are calculated directly from equation (C11) and converted into the S-wave effective parameters $V_{S0}^{\Sigma(P)}$, $V_{Sn}^{\Sigma(P)}$ by equations (10) and (19). The S-wave effective parameters $V_{S0}^{\Sigma(S)}$, $V_{Sn}^{\Sigma(S)}$, η_S^{Σ} are calculated with equation (28) and converted into the P-wave effective parameters $V_{P0}^{\Sigma(S)}$, $V_{Pn}^{\Sigma(S)}$ by equations (10) and (19).

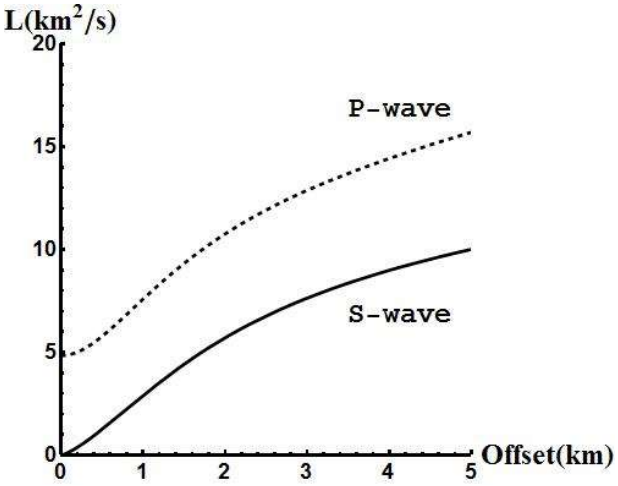

Figure 7 The relative geometrical spreading curves for an acoustic VTI medium with parameters shown in Table 1.

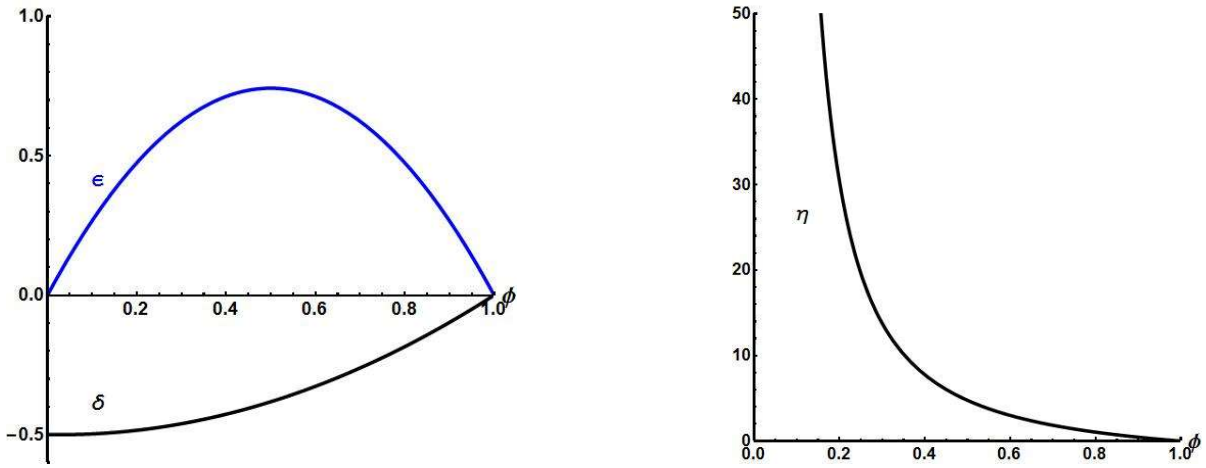

(a) (b)

Figure A1 The Thomsen's parameters ε, δ and their combination η as the function of fluid volume fraction in a binary medium.